RSC Advances

ROYAL SOCIETY OF CHEMISTRY

www.rsc.org/advances

Catalytic Oxidation of CO by N_2O on the Neutral Y_2MO_5 (M = Y, Al) Clusters: A Density Functional Theory Study

Hong-Ling Fang[a], Lei Xu[a], Jia Li[a], Bin Wang[a], Yong-Fan Zhang[a,b,c]*, Xin Huang[a,b]*

[a]*College of Chemistry, Fuzhou University, Fuzhou, Fujian 350116, PR China*

[b]*Fujian Provincial Key Laboratory of Theoretical and Computational Chemistry, Xiamen, Fujian 361005, PR China*

[c]*State Key Laboratory of Photocatalysis on Energy and Environment, Fuzhou University, Fuzhou, 350002, PR China*

*Corresponding author. Tel.: +86 591 22866139; fax: +86 591 22866156.
E-mail address: zhangyf@fzu.edu.cn (Y. F. Zhang); xhuang@fzu.edu.cn (X. Huang)

Abstract

Density functional theory (DFT) calculations are employed to investigate the full catalytic cycle of CO oxidation by N_2O on yttrium oxide clusters Y_2MO_5 (M = Y, Al) in gas-phase. Extensive structural searches show that both the ground-state structures of Y_3O_5 and Y_2AlO_5 contain an oxygen radical ($O_t^{\bullet}$) which plays an important role in CO oxidation. Energy profiles are calculated to determine the reaction mechanisms. Molecular electrostatic potential maps (MEPs) and natural bond orbital (NBO) analyses are employed to rationalize the reaction mechanisms. The results indicate that the whole catalytic cycle for the reaction $CO + N_2O \rightarrow CO_2 + N_2$, conducted by yttrium oxide clusters Y_2MO_5 (M = Y, Al), is favored both thermodynamically and kinetically. Moreover, compared with the previous report on di-nuclear $YAlO_3^{+\bullet}$ and $Y_2O_3^{+\bullet}$, it's obvious to conclude that tri-nuclear Y_3O_5 and Y_2AlO_5 exhibit greatly enhanced catalytic activity toward CO/N_2O couple.

Keywords: Density functional calculation; Yttrium oxide cluster; Oxygen radical center; Catalytic oxidation reaction; Doping effect

1. Introduction

Catalytic oxidation of harmful gases, such as carbon monoxide (CO) into carbon dioxide (CO_2) and nitrous oxide (N_2O) into nitrogen (N_2), is of great importance both environmentally and economically[1–10]. Even though oxidation of CO by N_2O is exothermic, they do not occur directly at any measurable temperatures because of high energy barrier for CO/N_2O couple[11]. It has been verified that some transition metal oxides are effective in catalytic oxidation of CO by N_2O[12–18]. Mechanistic investigation on the oxygen atom transfer process mediated by transition metal oxides which are involved in CO oxidation by N_2O is meaningful to design better catalysts with high activity and selectivity. Gas-phase cluster study has been emerged as an alternative approach to provide molecular-level insights into the complex chemical reaction processes occurring on the bulk transition metal oxide[19–28].

The catalytic oxidation of CO by N_2O at room temperature (RT) in the gas phase was demonstrated for the first time by Kappes and Staley with FeO^+ as a catalyst[12]. In the ensuing decades, numerous relevant investigations were developed subsequently[13–16]. For example, Castleman and co-workers have reported that a series of zirconium oxide $(ZrO_2)_x^+$ (x = 2–5) cations as well as $(Zr_xO_{2x+1})^-$ (x = 1–4) anions exhibit high activity in CO oxidation and the oxygen radical center with elongated zirconium-oxygen bond is the active site[13–15]. They also have shown that the initial zirconium oxide ions can be regenerated by treating oxygen-deficient zirconium-oxide clusters with N_2O. Besides, binary neutral metal oxide clusters $ZrScO_4$ and $ZrNbO_5$ were demonstrated to have similar reactivity with their isoelectronic ions $Zr_2O_4^+$ and $Zr_2O_5^-$ for CO oxidation and N_2O reduction[16]. Some other metal-oxide clusters, such as $Ce_mO_{2m}^+$ (m = 2–6), $Ce_nO_{2n+1}^-$ (n = 4–21), $(TiO_2)_nO^-$ (n = 3–25) and VO_3, were also exploited to bring out their oxidizing capacity towards CO[29–32]. These investigations have indicated the oxygen radical center plays a critical role in CO oxidation process.

Yttrium oxides are also promising for the catalytic application, yet the related studies on CO oxidation by yttrium oxides are relatively scarce[11,33]. Many early

studies have focused their attentions on the electronic structure and bonding of yttrium oxide clusters for their unique properties[34–38]. The previous study has pointed out that the $YAlO_3^{+\bullet}$ cluster contains oxygen radical center and shows better reactivity than homonuclear yttrium oxide cluster $Y_2O_3^{+\bullet}$ in CO oxidation[11]. Recently, the terminal oxygen radical was also found in the neutral Y_3O_5 cluster[38].

In this work, we present our theoretical study on CO oxidations by neutral Y_2MO_5 (M = Y, Al) clusters employing density functional calculations. Extensive structural searches show that both Y_3O_5 and Y_2AlO_5 clusters are doublet state with a single unpaired electron located on the terminal oxygen atom. The energy profiles are calculated to get the detail mechanisms underlying the oxygen atom transfer processes involved in CO oxidation reaction. Qualitative explanation for the reactions of Y_2MO_5 (M = Y, Al) clusters with CO can be understood from the molecular electrostatic potential maps and natural bond orbital analyses. The regenerations of Y_2MO_5 (M = Y, Al) clusters via the reactions of oxygen-deficient clusters Y_2MO_4 (M = Y, Al) with N_2O are also calculated. A full catalytic cycle for the reaction of CO with N_2O on Y_2MO_5 (M = Y, Al) clusters is thus complete.

2. Computational Methods

The theoretical calculations were performed at the DFT level using the BP86 functional[39,40]. The calculations were performed using analytical gradients with the Stuttgart relativistic small core basis set and efficient core potential[41,42]augmented with two *f*-type and one *g*-type polarization functions for yttrium [$\zeta(f) = 0.144, 0.546$; $\zeta(g) = 0.249$] as recommended by Martin and Sundermann[43] and the aug-cc-pvTZ basis set for oxygen, alumina, carbon and nitrogen[44,45]. Scalar relativistic effects, that is, the mass velocity and Darwin effects, were taken into account via the quasi-relativistic pseudopotentials. All the structures presented in the calculated energy profiles were fully optimized. The initial structures of the transition state were obtained by potential energy surface scans with appropriate coordinates. Vibrational frequency calculations were performed at the same level of theory to verify the nature

of the stationary points as minima (zero imaginary frequency) or transition states (one imaginary frequency). The pathways of the reaction mechanisms were further confirmed by intrinsic reaction coordinate (IRC) calculations[46,47].

The relative energies of the low-lying Y_2MO_x (M = Y, Al; x = 4–5) structures were further evaluated via single-point calculations at the coupled cluster [CCSD(T)][48–52] level with the Y/Stuttgart+2*f*1*g*/O/Al/aug-cc-pVTZ basis sets at the BP86 geometries. The results are summarized and available in Supplementary Material (Table S1). In our current studies, the BP86 gave superior results in terms of energies when directly compared to the results of CCSD(T) calculations. The previous studies on yttrium oxide clusters[38,53] also have indicated that the BP86 calculations can give good consistency with the experimental results. As discussed below, we used the results with the BP86 functional for further discussion. All DFT calculations were performed with the Gaussian 09 software package[54] and the CCSD(T) calculations were done using MOLPRO 2010.1 package[55]. Natural bond orbital (NBO) analysis was performed by using the NBO 3.1 program[56]. Three-dimensional molecular structures were visualized using the GaussView 4.1[57]. Three-dimensional contours of the molecular orbitals were visualized using the VMD software[58].

3. Results and Discussions

3.1 The structures and spin density analyses of Y_2MO_x (M = Y, Al; x = 4–5)

The optimized ground state structures and low-lying isomers within 0.40 eV for the neutral Y_3O_x and Y_2AlO_x (x = 4–5) clusters at the BP86 level are presented in Figs. 1–2. Alternative optimized geometries are shown in the Supplementary Information (Figs. S1–S2). In the following discussions, O_t, O_b and O_c stand for the terminal, bridging and capped oxygen atoms, respectively. The spin density analyses are performed to shed light on the nature of the radical character of these neutral ground states, as shown in Fig. 3.

Y_3O_4 and Y_3O_5

In the previous work, we have reported the structures of Y_3O_4 and Y_3O_5 clusters[38]. The low-lying isomers within 0.40 eV for Y_3O_4 and Y_3O_5 are given in Fig. 1. The ground state of Y_3O_4 is a doublet state C_{3v} ($^2A_1$) structure (Fig. 1a), which can be regarded as an umbellate structure with a capped oxygen atom and three bridging oxygen atoms. In our calculation, the bond lengths of $Y–O_c$ and $Y–O_b$ are 2.174 Å and 2.048 Å, respectively. Alternative optimized structures are located remarkably higher in energy (Figs. S1a–c).

The ground state of Y_3O_5 has a propensity to adopt a doublet ($^2A''$) state with C_s symmetry (Fig. 1b) at the BP86 level. The $Y–O_t$ bond length is 2.155 Å and can be considered as Y–O single bond. Two kinds of connection between caped oxygen and yttrium atoms are found in this structure, where the $Y–O_c$ distances are presented to be 2.134 Å and 2.309 Å, respectively. Two ($^2A'$) state structures showing in Fig. 1c and Fig. 1d are calculated to be 0.11 eV and 0.21 eV above the ground state, respectively. We also calculated the higher symmetry structure (D_{3h}) with two triply-bridging O atoms and three doubly-bridging O atoms for Y_3O_5, which converged to the C_s structure, as shown in Fig. 1d. The relative energies for these low-lying structures (within ~ 0.20 eV) were further evaluated using single point CCSD(T) calculations. The results of CCSD(T) calculations are in line with those of DFT calculations.

Y_2AlO_4 and Y_2AlO_5

We carried out extensive structural searches for the ground-state structures on the potential energy surfaces of Y_2AlO_4 and Y_2AlO_5 clusters considering a variety of structural candidates including different spin states and geometries. The global minimum of Y_2AlO_4 is predicted to be a doublet state ($^2A'$) with C_s symmetry (Fig. 2a), which shows resemblance with Y_3O_4 (C_{3v}, $^2A_1$) in geometry (Fig. 1a). The low-lying isomer C_{2v} ($^2A_1$) (Fig. 2b) with four bridging O atoms is only 0.02 eV above the global minimum at BP86 level. Single-point CCSD(T) calculations were performed for these two isomers, revealing that the (C_s, $^2A'$) structure (Fig. 2a) is 0.12 eV more stable than the (C_{2v}, $^2A_1$) structure (Fig. 2b).

As for Y_2AlO_5, selected optimized structures with their relative energies are given in Figs. 2c–f. The ground state of Y_2AlO_5 is a doublet state C_s (^{2}A") as shown in Fig. 2c. It can be viewed that the Al atom replaces the yttrium atom which is link with the terminal oxygen atom in Y_3O_5. The Al–O_t distance is 1.767 Å and can be labeled as Al–O single bond[59]. The (^{2}A') state with similar geometry is 0.12 eV above the ground state at the BP86 level. The C_{2v} ($^2B_2$) (Fig. 2d) and C_{2v} ($^2B_1$) (Fig. 2f), which own a terminal and four bridging oxygen atoms, are 0.08 eV and 0.31 eV higher in energy, respectively. These low-lying structures within 0.20 eV were further evaluated by CCSD(T) calculations and the isomer (C_s, ^{2}A") (Fig. 2c) is still the lowest-energy structure.

Spin density analysis

All the ground states of Y_2MO_x (M = Y, Al; x = 4–5) clusters are doublet state. As mentioned above, the global minimum of Y_3O_4 is a C_{3v} structure with a capped and three bridging oxygen atoms. The spin is distributed equally on three yttrium atoms, as shown in Fig. 3a. After doping an aluminum atom, the unpaired electron is mainly located on aluminum atom in Y_2AlO_4 (Fig. 3b). Both Y_3O_5 and Y_2AlO_5 clusters contain an oxygen radical ($O^\bullet$) as depicted in Fig. 3c and Fig. 3d, respectively. The singly occupied molecular orbitals (SOMOs) of Y_3O_5 and Y_2AlO_5 (Fig. 4) indicate that the unpaired electron is located on the 2*p* orbitals of terminal oxygen atom.

To our knowledge, the oxygen-centre radical is highly reactive. It's able to oxidize a variety of stable molecules including CO and many small organic species at low temperature, such as CH_4, C_2H_4, C_2H_2 and so forth[14,60–63]. He and co-workers have studied the reactions of CO with $Y_2O_3^{+\bullet}$ and $YAlO_3^{+\bullet}$ by mass spectrometry and density functional theoretical[11]. According to their results, oxidation of the CO by $Y_2O_3^{+\bullet}$ is prevented by an energy barrier, while oxidation of the CO with $YAlO_3^{+\bullet}$ is favored. The differences are mainly produced by the spin distributions. In $Y_2O_3^{+\bullet}$, the unpaired electron is delocalized over three bridging oxygen atoms. As for $YAlO_3^{+\bullet}$, the spin is mainly located on the terminal oxygen atom of Al–$O_t^\bullet$ unit. However, the

single unpaired electrons of Y_3O_5 and Y_2AlO_5 clusters both located on the terminal oxygen atom of $M–O_t^{\bullet}$ (M = Y, Al) subunit. In the next section, the mechanisms for CO oxidation by Y_3O_5 and Y_2AlO_5 are presented.

3.2 The reactions of Y_2MO_5 (M = Y, Al) with CO

The detail mechanisms for the reactions of Y_2MO_5 (M = Y, Al) with CO are investigated at the BP86 level. In our calculation, all the intermediates and transition structures in doublet state are much more stable than those in quartet state. So DFT calculations are performed for the molecule reactions of Y_2MO_5 (M = Y, Al) towards CO on the doublet ground state potential energy surfaces. The products are proposed according to the following equations:

$$Y_2MO_5\,(M = Y, Al) + CO \rightarrow Y_2MO_4\,(M = Y, Al) + CO_2$$

We have considered the possible paths for the reactions and found the way in which CO reacts with the $M–O_t^{\bullet}$ site is more preferred. Then we will focus on the mechanism for CO oxidation involving the oxygen radical center. Figs. 5–6 present the favored energy profiles calculated at the BP86 level in which IM*n* represent the intermediate structures and TS*n* correspond to the transition states, respectively. The detail of electron transfer procedures can be obtained by analyzing the spin density of the intermediates and transition states in the reactions as shown in Figs. S8–S9. The Cartesian coordinates for the optimized structures on the potential energy surfaces are given in Table S3. Other possible reaction paths were also calculated and given in Figs. S3–S7.

3.2.1 The reaction profiles of Y_2MO_5 (M = Y, Al) with CO

Y_3O_5 with CO

The calculated energy profile for the reaction between Y_3O_5 and CO is presented in Fig. 5. The oxidation reaction occurs through the exothermic (0.29 eV) binding of the carbon atom of CO to the radical oxygen and the adjacent yttrium atom of Y_3O_5 forming an intermediate (IM1). In IM1, the distances of carbon atom to yttrium atom and the radical oxygen are 2.699 Å and 2.749 Å, respectively. Formation of the IM2

requires a transfer of spin from the terminal oxygen to the nonlinear CO_2 unit. This involves an easily surmountable barrier of 0.02 eV. In the process, the C–O_t distance decreases from 2.749 Å to 1.275 Å and Y–O_t length increases by 0.138 Å. From IM2, the nonlinear CO_2 subunit rotates around the Y–O_t bond involving a transition state (TS2) which is 0.10 eV higher in energy. The resulting complex IM3 is lower in energy by 2.64 eV than the reactants. There is another transition state (TS2') from IM2 to IM3, which needs to overcome 0.54 eV of barrier, as shown in Fig. S3. The unpaired electron transfers from the curving bent CO_2 motif back to the yttrium oxide cluster needs to overcome a barrier of 0.61 eV through the transition state (TS3). In this process, the distance of the terminal oxygen atom to the adjacent yttrium atom is elongated, that is, 2.325 Å for IM3, 2.510 Å for TS3 and 2.589 Å for IM4, respectively. The IM4 is 2.05 eV lower in energy than the reactants with a linear CO_2. Finally, dissociation of CO_2 from IM4 to form the products Y_3O_4 and CO_2 requires 0.25 eV of energy. The overall oxidation reaction is barrierless and calculated to be exothermic by 1.80 eV, indicating the oxidation reaction is favorable both kinetically and thermodynamically.

Y_2AlO_5 with CO

The calculated energy profile of Fig. 6 shows that the reaction of Y_2AlO_5 with CO proceeds according to a general mechanism involving the initial binding of the carbon atom of CO to the radical oxygen of Y_2AlO_5. The initial encounter complex IM1 is 2.11 eV more stable than the reactants and contains a bent CO_2 subunit that results from the transfer of single unpaired electron to CO. The bond lengths of C–O_t and Al–O_t are 1.314 Å and 1.800 Å, respectively. In the following steps, the CO_2 moiety is transferred from the Al site to the Y site of Y_2AlO_4 subunit, involving the transitions which are 0.54 eV and 0.53 eV higher in energy for TS1 and TS2, respectively. IM2 and IM3 are 2.34 eV and 2.20 eV lower in energy than the separated reactants, respectively. Spin density is appeared to be mainly located on the Y_2AlO_4 subunit for the IM2 and Al atom for IM3, respectively (Fig. S9). With the increase of the distance from the carbon atom to the bridge oxygen atom and the

decrease of the distance from the carbon atom to the capped oxygen atom, the CO_2 subunit is passed to the Y–O_c site forming IM4, requiring an energy barrier of 0.53eV through the TS3. The CO_2-absorbing (CO_2 ready-desorbing) IM4 is 1.70 eV lower in energy than the reactants. Besides, the electron located on CO_2 unit of IM1 can directly transfer to Al atom forming the IM4 with a barrier of 1.28 eV, as depicted in Fig. S5. Finally, loss of the CO_2 from IM4 requires 0.31 eV of energy, and the overall process is exothermic by 1.39 eV, resulting in Y_2AlO_4 and CO_2 products.

3.2.2 The molecular electrostatic potential and natural bond orbital analyses

An additional supporting finding for the reactions is acquired by considering the molecular electrostatic potential maps (MEPs) and natural bond orbital (NBO) analyses. As can be seen in Fig. S10 for Y_3O_5 cluster, the MEP exhibits positive values (the blue areas) which are preferred for CO-adsorption. In our calculations, the way that CO adsorbs on the yttrium atom featured by terminal oxygen atom is preferred both kinetically and thermodynamically. In contrast, CO binding to the yttrium atoms which connect with the capped oxygen and bridging oxygen atoms is impeded by an energy barrier, as shown in Fig. S4. Just as many researchers have reported, metal atom adjacent to the oxygen-centered radical is more reactive toward CO[16,29]. The MEP of Y_2AlO_5 is positive over two yttrium atoms surface. However, the way that CO adsorbs on the yttrium atoms of the Y_2AlO_5 cluster is not favored as depicted in Fig. S7. In Y_2AlO_5, the oxygen radical center area is relatively negative. Attacking at the oxygen radical center leads to the oxidation reaction, which is a preferable path without any energy barrier as shown previously[14,16,17].

The MEP of CO_2 molecular, shown in Fig. S10, is positive over carbon atom and negative over oxygen atoms, respectively. In Y_3O_4, the yttrium atoms are the most positive (1.74|e|) sites and the capped oxygen is more negative (–1.34|e|) than bridging oxygen sites. Therefore, the linear CO_2 has a tendency to split from the Y–O_c bond. Analogously, the yttrium site (1.91|e|) is more positive than aluminum site (1.47|e|) in Y_2AlO_4, which may explain why the CO_2 molecular dissociates from the Y–O_c bond rather than Al–O_c bond.

3.3 The reaction of Y_2MO_4 (M = Y, Al) with N_2O

The Y_2MO_5 (M = Y, Al) clusters can be retrieved by treating Y_2MO_4 (M = Y, Al) clusters with N_2O. Then a full cycle is attainable in the reactions of CO with N_2O by neutral Y_2MO_5 (M = Y, Al) clusters (Fig. 7). DFT calculations at the BP86 level are performed for the reactions of Y_2MO_4 (M = Y, Al) with N_2O. The favorite paths for Y_3O_4 and Y_2AlO_4 towards N_2O are presented in Figs. 8–9, respectively. The others listed in the supplementary information (Figs. S11–S12).

Y_3O_4 with N_2O

The calculated energy profile for the reaction between Y_3O_4 and N_2O is presented in Fig. 8. For Y_3O_4, the spin is delocalized equally over the three yttrium atoms. The adsorption of N_2O on the equivalent yttrium atom leads to the intermediate (IM1), which is 1.35 eV more stable than the reactants. With the increase of the distance between O atom and N atom (1.399 *to* 2.789 Å) and the decrease of the distance from O atom to Y atom (2.275 *to* 2.172 Å), the O atom is passed on smoothly to bind with Y atom forming IM2. The activation barrier of the oxygen transfer is calculated to be 0.05 eV, which corresponds primarily to the breaking of the bond of N–O. The IM2 is 1.68 eV lower in energy than the reactants. Dissociation of the N_2 unit generates the products Y_3O_5 and N_2, which requires 0.01 eV of energy. The total oxidation reaction is exothermic by 1.67 eV.

Y_2AlO_4 with N_2O

The possible paths for the Y_2AlO_4 cluster reducing N_2O are displayed in Fig. 9 and Figs. S11–S12. The current study shows that the unpaired electron in Y_2AlO_4 cluster mainly located on the main-group metal aluminum atom. As the N_2O molecule attacking the aluminum atom, the unpaired electron will occupy the LUMO anti-bonding orbital of N_2O and the N–O distance will be lengthened to 2.824 Å. The interaction of the Al atom and N_2 unit is weak as their distance is 2.643 Å. The complex IM1 is 1.99 eV more stable than the separated reactants. Releasing the N_2 from IM1 is rather easy without any barrier. The overall process is barrier-less and calculated to be exothermic by 2.09 eV.

The different reactivity of Y_3O_4 versus Y_2AlO_4 in their reactions with N_2O is just another example of the role spin distributions often played in chemical reactions. In the doped Y_2AlO_4, the unpaired electron is mainly localized on the Al atom, while in the homonuclear Y_3O_4 cluster, the spin delocalized equally over the three bridging Y atoms. Consequently, the reaction patterns of Y_3O_4 and Y_2AlO_4 towards N_2O are different. Furthermore, the different spin distributions also induce a more negative change of Gibbs free energy for Y_2AlO_4 (−2.14 eV) in reacting with N_2O than that of Y_3O_4 (−1.79 eV). In other words, while doping a main group Al atom the reaction is favorable both thermodynamically and kinetically.

3.4 Comparison with di-nuclear yttrium oxide clusters

As mentioned above, the reactions of CO with Y_2MO_5 (M = Y, Al) are barrierless and exothermic, and the other half of the catalytic cycles for regenerations of Y_2MO_5 (M = Y, Al) by N_2O are favored both thermodynamically and kinetically. Thus the full catalytic cycle is attainable in this work. The catalytic ability of di-nuclear yttrium oxides clusters $Y_2O_3^{+\bullet}$ and $YAlO_3^{+\bullet}$ for CO/N_2O couple also have been studied by He and co-workers[11]. The oxidation of CO with $Y_2O_3^{+\bullet}$ is impeded by an energy barrier. As one yttrium atom of $Y_2O_3^{+\bullet}$ was replaced by one aluminum atom, the oxygen radical center was generated leading to the reaction barrier-less. Regeneration of $YAlO_3^{+\bullet}$ from $YAlO_2^{+\bullet}$ with N_2O dose not take place and the catalytic cycle cannot be closed. Combined our calculations with He et al report, it's obvious to conclude that the tri-nuclear yttrium oxides clusters exhibit greatly enhanced catalytic activity in the reaction of CO with N_2O.

4. Conclusion

Extensive DFT calculations are employed to investigate the reaction mechanism of CO oxidation by Y_2MO_5 (M = Y, Al) clusters and the regeneration of Y_2MO_5 (M = Y, Al) clusters using N_2O. Theoretical investigations reveal that both the Y_3O_5 and Y_2AlO_5 clusters are doublet state with a single unpaired electron located on the terminal oxygen atom. Calculated energy profiles for the reactions of Y_3O_5 and

Y_2AlO_5 with CO are energetically favorable and barrierless. The high reactivity for Y_2MO_5 clusters is ascribed to the oxygen radical center. The reaction mechanisms for Y_2MO_5 (M = Y, Al) clusters with CO may be understood qualitatively from the molecular electrostatic potential maps and natural bond orbital analyses. Regenerations of the initial species Y_2MO_5 (M = Y, Al) by N_2O constitute the other half of the catalytic cycle. Based on the previous study of di-nuclear $YMO_2^{+\bullet}$ (M = Y, Al), we propose that by controlling the cluster size (or doping ratio), it's possible to generate neutral oxide cluster with localized radical oxygen center, which is highly active in redox reations.

Acknowledgments

This work was supported by the National Natural Science Foundation of China (21371034, 21373048 and 21301030), the Natural Science Foundation of Fujian Province for Distinguished Young Investigator Grant (2013J06004), and the Independent Research Project of State Key Laboratory of Photocatalysis on Energy and Environment (2014A02).

Supplementary Information Available

The others possible pathways for the redox reaction are presented in Figs. S3–S7 and Figs. S11–S12. Numerical electron spin density (in |e|) for the structures presented in the energy profiles of Figs. 5–6 are shown in Figs. S8–S9. The Cartesian coordinates for the reactants, intermediates, transition states and the products shown in the energy profiles of Figs. 5–6, Figs. 8–9 are listed in Table S3.

References

1 A. R. Ravishankara, J. S. Daniel and R. W. Portmann, *Science*, 2009, **326**, 123.

2 B. K. Min and C. M. Friend, *Chem. Rev.*, 2007, **107**, 2709.

3 S. Royer and D. Duprez, *Chem. Cat. Chem.*, 2011, **3**, 24.

4 S. J. Lin, J. Cheng, C. F. Zhang, B. Wang, Y. F. Zhang and X. Huang, *Phys. Chem. Chem.*

Phys., 2015, **17**, 11499.

5 I. Lopes, A. Davidson and C. Thomas, *Catal. Commun.*, 2007, **8**, 2105.

6 G. W. Peng, L. R. Merte, J. Knudsen, R. T. Vang, E. Lagsgaard, F. Besenbacher and M. Marvrikakis, *J. Phys. Chem. C*, 2010, **114**, 21579.

7 X. W. Xie, Y. Li, Z. Q. Liu, M. Haruta and W. J. Shen, *Nature*, 2009, **458**, 746.

8 H. J. Freund, G. Meijer, M. Scheffler, R. Schlogl and M. Qolf, *Angew. Chem. Int. Ed.*, 2011, **50**, 10064.

9 W. E. Kaden, W. A. Kunkel, F. S. Roberts, M. Kane and S. L. Andersona, *J. Chem. Phys.*, 2012, **136**, 204705.

10 O. P. Balaj, I. Balteanu, T. T. J. Roβteuscher, M. K. Beyer and V. E. Bondybey, *Angew. Chem. Int.*
Ed., 2004, **43**, 6519.

11 J. B. Ma, Z. C. Wang, M. Schlangen, S. G. He and H. Schwarz, *Angew. Chem. Int. Ed.*, 2013, **52**, 1226.

12 M. M. Kappes and R. H. Staley, *J. Am. Chem. Soc.*, 1981, **103**, 1286.

13 G. E. Johnson, R. Mitrić, E. C. Tyo, V. Bonačić-Koutecký and A. W. Castleman, Jr., *J. Am. Chem. Soc.*, 2008, **130**, 13912.

14 G. E. Johnson, R. Mitrić, M. Nössler, E. C. Tyo, V. Bonačić-Koutecký and A. W. Castleman, Jr., *J. Am. Chem. Soc.*, 2009, **131**, 5460.

15 G. E. Johnson, R. Mitrić, V. Bonačić-Koutecký and A. W. Castleman, Jr., *Chem. Phys. Lett.*, 2009, **475**, 1.

16 M. Nößler, R. Mitrić, V. Bonačić-Koutecký, G. E. Johnson, E. C. Tyo and A. W. Castleman, Jr., *Angew. Chem. Int. Ed.*, 2010, **49**, 407.

17 Z. C. Wang, N. Dietl, R. Kretschmer, T. Weiske, M. Schlangen and H. Schwarz, *Angew. Chem. Int. Ed.*, 2011, **50**, 12351.

18 E. C. Tyo, M. Nößler, R. Mitrić, V. Bonačić-Koutecký and A. W. Castleman, Jr., *Phys. Chem. Chem. Phys.*, 2011, **13**, 4243.

19 A. W. Castleman, Jr., *Catal. Lett.*, 2011, **141**, 1243.

20 S. Yin and E. R. Bernstein, *Int. J. Mass Spectrom.*, 2012, **321–322**, 49.

21 S. M. Lang and T. M. Bernhardt, *Phys. Chem. Chem. Phys.*, 2012, **14**, 9255.

22 K. R. Asmis, *Phys. Chem. Chem. Phys.*, 2012, **14**, 9270.

23 H. Schwarz, *Angew. Chem. Int. Ed.*, 2011, **50**, 10096.

24 M. Schlangen and H. Schwarz, *Catal. Lett.*, 2012, **142**, 1265.

25 Z. C. Wang, N. Dietl, R. Kretschmer, J. B. Ma, T. Weiske, M. Schlangen and H. Schwarz, *Angew. Chem. Int. Ed.*, 2012, **51**, 3703.

26 Z. C. Wang, X. N. Wu, Y. X. Zhao, J. B. Ma, X. L. Ding and S. G. He, *Chem. Eur. J.*, 2011, **17**, 3449.

27 Z. C. Wang, T. Weiske, R. Kretschmer, M. Schlangen, M. Kaupp and H. Schwarz, *J. Am.*

Chem. Soc., 2011, **133**, 16930.

28 Z. C. Wang, X. N. Wu, Y. X. Zhao, J. B. Ma, X. L. Ding and S. G. He, *Chem. Phys. Lett.*, 2010, **489**, 25.

29 X. N. Wu, Y. X. Zhao, W. Xue, Z. C. Wang, S. G. He and X. L. Ding, *Phys. Chem. Chem. Phys*., 2010, **12**, 3984.

30 X. N. Wu, X. L. Ding, S. M. Bai, B. Xu, S. G. He and Q. Shi, *J. Phys. Chem. C*, 2011, **115**, 13329.

31 J. B. Ma, B. Xu, J. H. Meng, X. N. Wu, X. L. Ding, X. N. Li and S. G. He, *J. Am. Chem. Soc.*, 2013, **135**, 2991.

32 Z. C. Wang, W. Xue, Y. P. Ma, X. L. Ding, S. G. He, F. Dong, S. Heinbuch, J. J. Rocca and E. R. Bernstein, *J. Phys. Chem. A*, 2008, **112**, 5984.

33 M. R. Sievers and P. B. Armentrout, *Inorg. Chem.*, 1999, **38**, 397.

34 M. Knickelbein, *Chem. Phys.*, 1995, **102**, 1.

35 A. Pramann, Y. Nakamura and A. Nakajima, *J. Phys. Chem. A*, 2001, **105**, 7534.

36 G. Gu, B. Dai, X. Ding and J. Yang, *Eur. Phys. J. D*, 2004, **29**, 27.

37 B. Dai, K. Deng and J. Yang, *Chem. Phys. Lett.*, 2002, **364**, 188.

38 L. Xu, C. J. Xia, L. F. Wang, L. Xie, B. Wang, Y. F. Zhang and X. Huang, *RSC Adv.*, 2014, **4**, 60270.

39 A. D. Becke, *Phys. Rev. A*, 1988, **38**, 3098.

40 J. P. Perdew, *Phys. Rev. B*, 1986, **33**, 8822.

41 W. Küchle, M. Dolg, H. Stoll and H. Preuss, Pseudopotentials of the Stuttgart/Dresden group 1998, revision August 11, 1998: http://www.theochem.uni-stuttgart.de/pseudopotentiale.

42 D. Andrae, U. Häeußermann, M. Dolg, H. Stoll and H. Preuss, *Theor. Chim. Acta.*, 1990, **77**, 123.

43 J. M. L. Martin and A. Sundermann, *J. Chem. Phys.*, 2001, **114**, 3408.

44 R. A. Kendall and T. H. Dunning, Jr., R. J. Harrison, *J. Chem. Phys.*, 1992, **96**, 6796.

45 T. H. Dunning, Jr., *J. Chem. Phys.*, 1989, **90**, 1007.

46 C. Gonzalez and H. B. Schlegel, *J. Chem. Phys.*, 1989, **90**, 2154.

47 C. Gonzalez and H. B. Schlegel, *J. Phys. Chem.*, 1990, **94**, 5523.

48 G. D. Purvis III and R. J. Bartlett, *J. Chem. Phys.*, 1982, **76**, 1910.

49 G. E. Scuseria, C. L. Janssen and H. F. Schaefer III, *J. Chem. Phys.*, 1988, **89**, 7382.

50 K. Raghavachari, G.W. Trucks, J.A. Pople and M. Head-Gordon, *Chem. Phys. Lett.*, 1989, **157**, 479.

51 J. D. Watts, J. Gauss and R. J. Bartlett, *J. Chem. Phys.*, 1993, **98**, 8718.

52 R. J. Bartlett and M. Musial, *Rev. Mod. Phys.*, 2007, **79**, 291.

53 Y. Gong, C. F. Ding and M. F. Zhou, *J. Phys. Chem. A*, 2009, **113**, 8569.

54 M. J. Frisch, G. W. Trucks, H. B. Schlegel, G. E. Scuseria, M. A. Robb, J. R. Cheeseman, G. Scalmani, V. Barone, B. Mennucci, G. A. Petersson, H. Nakatsuji, M. Caricato, X. Li, H. P.

Hratchian, A. F. Izmaylow, J. L. Sonnenberg, M. Hada, M. Ehara, K .Toyota, R. Fukuda, J. Hasegawa, M. Ishida, T. Nakajima, Y. Honda, O. Kitao, H. Nakai, T. Vreven, J. A. Montgomery, Jr., J. E. Peralta, F. Ogliaro, M. Bearpark, J. J. Heyd, E. Brothers, K. N. Kudin, V. N. Staroverov, R. Kobayashi, J. Normand, K. Raghavachari, A. Rendell, J. C. Burant, S. S. Iyengar, J. Tomasi, M. Cossi, N. Rega, J. M. Millam, M. Klene, J. E. Knox, J. B. Cross, V. Bakken, C. Adamo, J. Jaramillo, R. Gomperts, R. E. Stratmann, O. Yazyev, A. J. Austin, R. Cammi, C. Pomelli, J. W. Ochterski, R. L. Martin, K. Morokuma, V. G. Zakrzewski, G. A. Voth, P. Salvador, J. J. Dannenberg, S. Dannenberg, S. Dapprich, A. D. Daniels, O. Farkas, J. B. Foresman, J. V. Ortiz, J. Cioslowski, and D. J. Fox, Gaussian 09, Revision A.1, Gaussian, Inc., Wallingford CT, 2009.

55 H. J. Werner, P. J. Knowles, F. R. Manby, M. Schütz, P. Celani, G. Knizia, T. Korona, R. Lindh, A. Mitrushenkov, G. Rauhut, T. B. Adler, R. D. Amos, A. Bernhardsson, A. Berning, D. L. Cooper, M. J. O. Deegan, A. J. Dobbyn, F. Eckert, E. Goll, C. HamPel, A. Hesselmann, G. Hetzer, T. Hrenar, G. Jansen, C. K?PPl, Y. Liu, A. W. Lloyd, R. A. Mata, A. J. May, S. J. McNicholas, W. Meyer, M. E. Mura, A. Nicklass, D. P. O'Neill, P. Palmieri, K. Pflüger, R. Pitzer, M. Reiher, T. Shiozaki, H. Stoll, A. J. Stone, R. Tarroni, T. Thorsteinsson, M. Wang and A. Wolf, MOLPRO, version 2010.1, a package of ab initio programs; See http://www.molpro.net.

56 E. D. Glendening, A. E. Reed, J. E. Carpenter and F. Weinhold, NBO Version 3.1.

57 R. Dennington II, T. Keith, J. Millam, K. Eppinnett, W. L. Hovell and R. Gilliland, GaussView: Version 4.1, Semichem Inc.: Shawnee Mission, KS, 2007.

58 W. Humphrey, A. Dalke and K. Schulten, *J. Mol. Graphics*, 1996, **14**, 33.

59 A. Martínez, F. J. TenorioJ and V. Ortiz, *J. Phys. Chem. A*, 2001, **105**, 11291.

60 Y. X. Zhao, X. N. Wu, J. B. Ma, S. G. He and X. L. Ding, *Phys. Chem. Chem. Phys.*, 2011, **13**, 1925.

61 J. B. Ma, Z. C. Wang, M. Schlangen, S. G. He and H. Schwarz, *Angew. Chem. Int. Ed.*, 2012, **51**,5991.

62 N. Dietl, M. Schlangen and H. Schwarz, *Angew. Chem. Int. Ed.*, 2012, **51**, 5544.

63 X. L. Ding, X. N. Ding, Y. X. Zhao and S. G. He, *Acc. Chem. Res.*, 2012, **45**, 382.

Fig. 1. Optimized global minima and selected low-lying structures (within ~0.40 eV) for Y_3O_x (x = 4–5) clusters at the BP86 level. The bond lengths are in angstroms.

Fig. 2. Optimized global minima and selected low-lying structures (within ~0.40 eV) for Y_2AlO_x (x = 4–5) clusters at the BP86 level. The bond lengths are in angstroms.

Fig. 3. Numerical electron spin density (in |e|) for the ground states of Y_2MO_x (M = Y, Al; x = 4–5) clusters.

Fig. 4. The singly occupied molecular orbitals for the ground states of Y_2MO_5 (M = Y, Al) clusters.

Fig. 5. DFT calculated energy profile for the reaction of Y_3O_5 cluster with CO_2. The reactants, intermediates, transition states and produces of the reaction are denoted as R, IM*n*, TS*n* and P, respectively. The energies (given in eV) are relative to the entrance channel. Some key bond lengths are given in angstroms.

Fig. 6. DFT calculated energy profile for the reaction of Y_2AlO_5 cluster with CO. The reactants, intermediates, transition states and produces of the reaction are denoted as R, IM*n*, TS*n* and P, respectively. The energies (given in eV) are relative to the entrance channel. Some key bond lengths are given in angstroms

Fig. 7. Proposed full catalytic cycle reaction involving CO and N_2O mediated by Y_2MO_5 (M = Y, Al) clusters.

Fig. 8. DFT calculated for the reaction of N_2O with Y_3O_4 cluster. The reactants, intermediates, transition states and produces of the reaction are denoted as R, IM*n*, TS*n* and P, respectively. The energies (given in eV) are relative to the entrance channel. Some key bond lengths are given in angstroms

Fig. 9. DFT calculated for the reaction of N_2O with Y_2AlO_4 cluster. The reactants, intermediates and produces of the reaction are denoted as R, IM1 and P, respectively. The energies (given in eV) are relative to the entrance channel.

Some key bond lengths are given in angstroms

Fig. 1

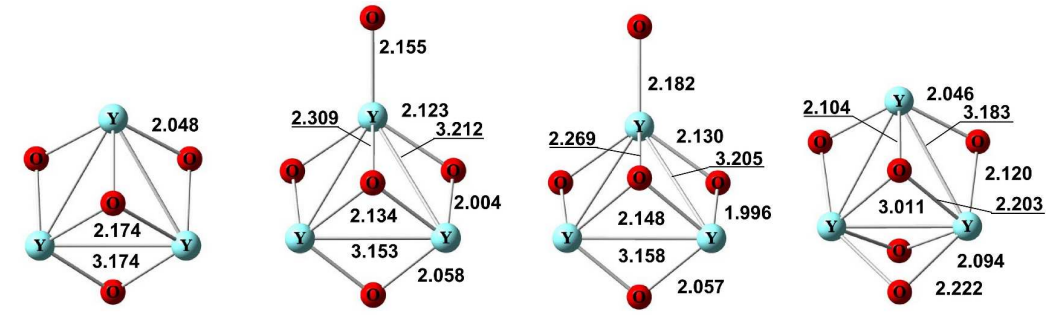

(a) Y_3O_4 C_{3v} ($^2A_1$ 0.00 eV) (b) Y_3O_5 C_s ($^2A''$ 0.00 eV) (c) Y_3O_5 C_s ($^2A'$ 0.11 eV) (d) Y_3O_5 C_s ($^2A'$ 0.21 eV)

Fig. 2

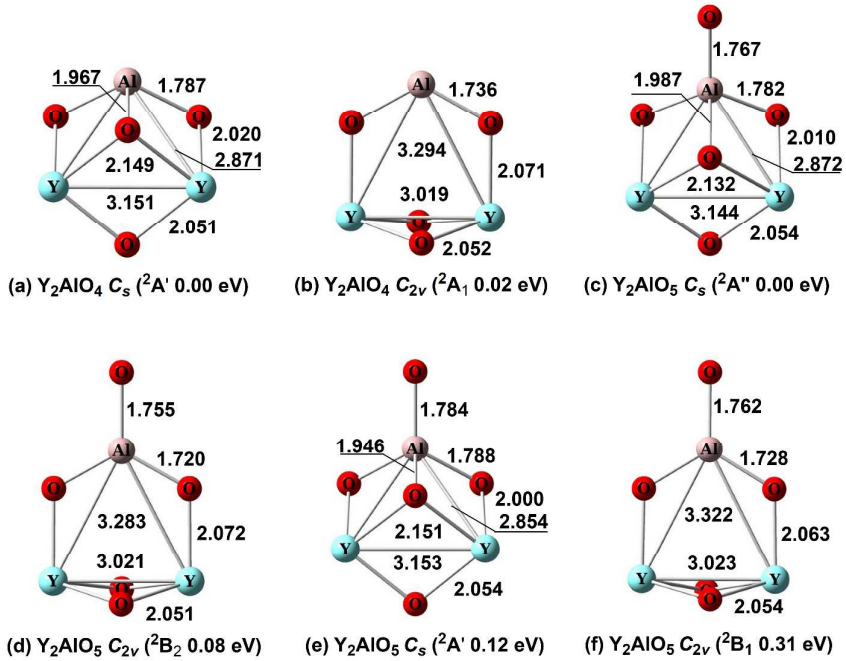

(a) Y_2AlO_4 C_s ($^2A'$ 0.00 eV) (b) Y_2AlO_4 C_{2v} ($^2A_1$ 0.02 eV) (c) Y_2AlO_5 C_s ($^2A''$ 0.00 eV)

(d) Y_2AlO_5 C_{2v} ($^2B_2$ 0.08 eV) (e) Y_2AlO_5 C_s ($^2A'$ 0.12 eV) (f) Y_2AlO_5 C_{2v} ($^2B_1$ 0.31 eV)

Fig. 3

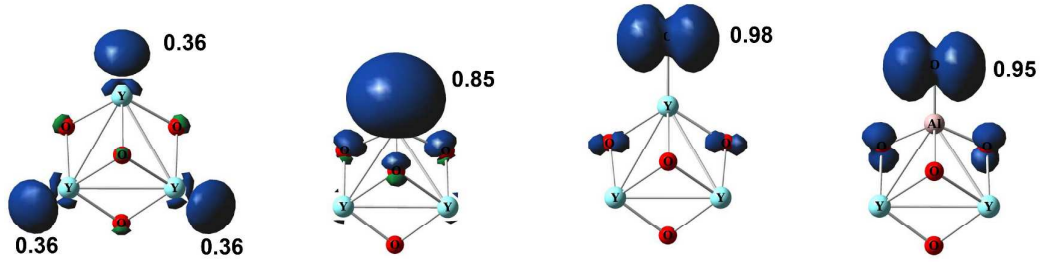

(a) Y_3O_4 C_{3v} ($^2A_1$) (b) Y_2AlO_4 C_s ($^2A'$) (c) Y_3O_5 C_s ($^2A''$) (d) Y_2AlO_5 C_s ($^2A''$)

Fig. 4

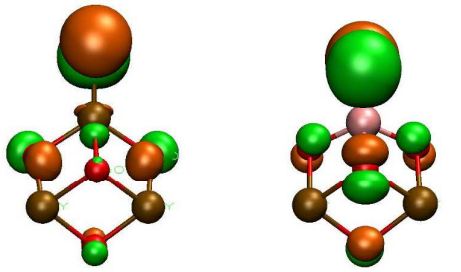

(SOMO) (SOMO)

(a)Y_3O_5 (C_s ^{2}A") (b) Y_2AlO_5 (C_s ^{2}A")

Fig. 5

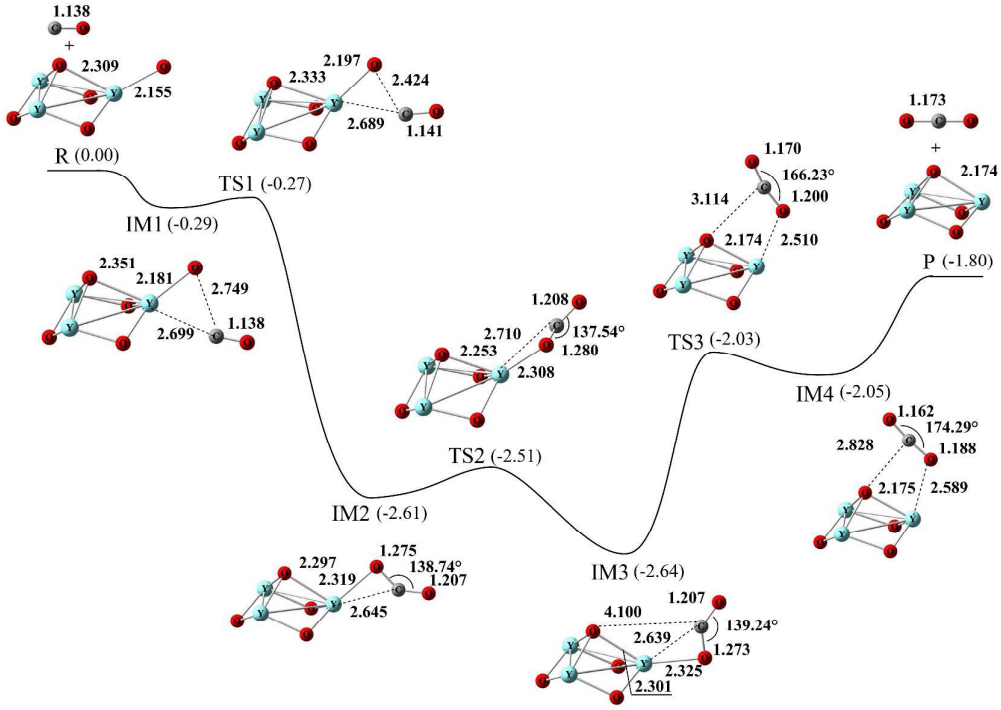

Fig. 6

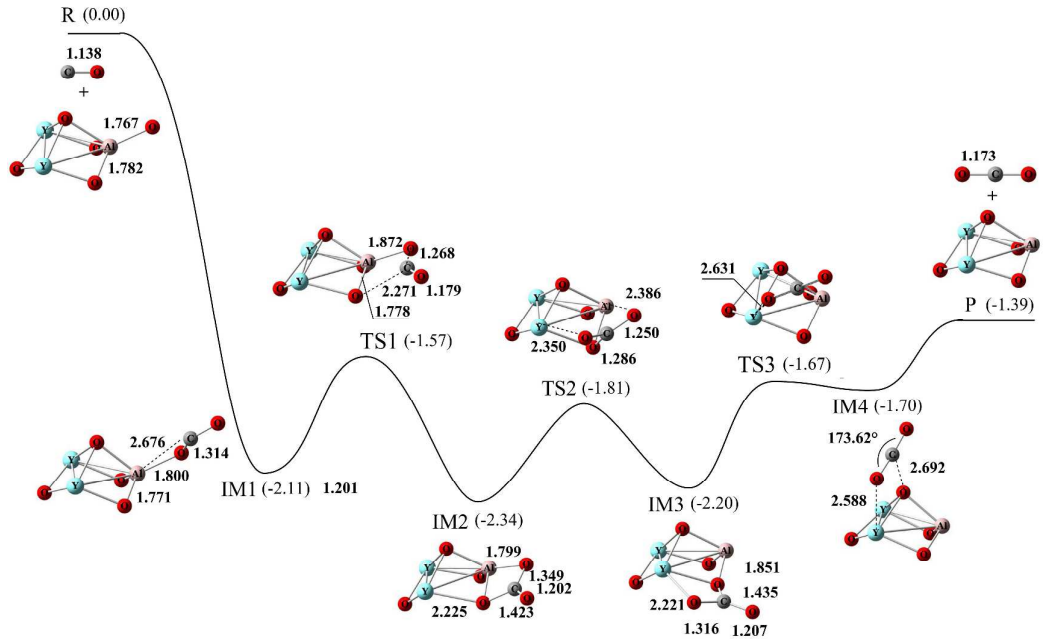

Fig. 7

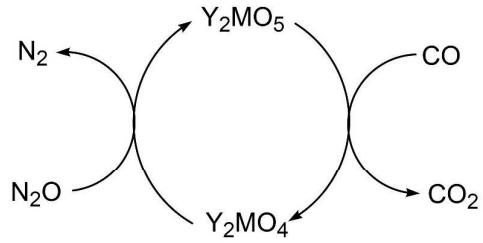

$$CO + N_2O \xrightarrow{Y_2MO_5\ (M = Y, Al)} CO_2 + N_2$$

Fig. 8

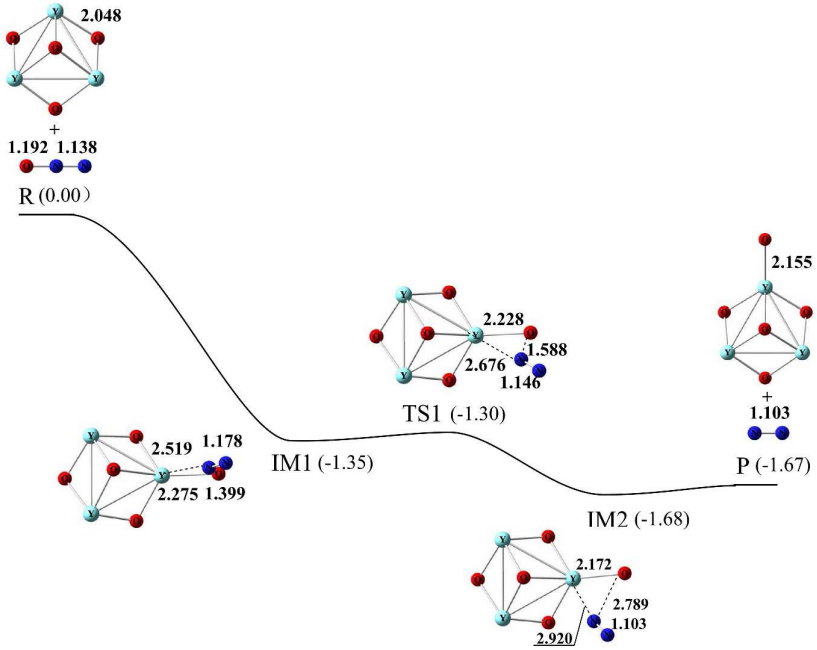

Fig. 9

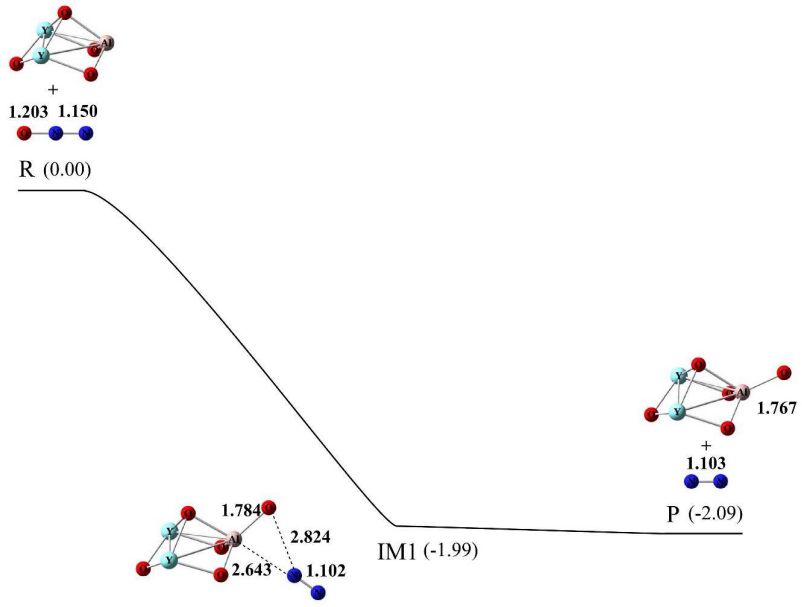

Catalytic Oxidation of CO by N_2O on the Neutral Y_2MO_5 (M = Y, Al) Clusters: A Density Functional Theory Study

Hong-Ling Fang[a], Lei Xu[a], Jia Li[a], Bin Wang[a], Yong-Fan Zhang[a,b,c]*, Xin Huang[a,b]*

Table of contents entry

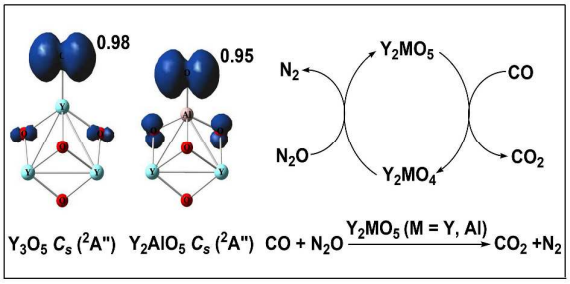

The full catalytic cycle of CO oxidation by N_2O on the neutral Y_2MO_5 (M = Y, Al) clusters has been studied in the current work.